Cross-regulation between CDK and MAPK control cellular fate

Eric Durandau, Serge Pelet*

Department of Fundamental Microbiology, University of Lausanne, CH-1015 Lausanne, Switzerland

* Corresponding author: serge.pelet@unil.ch

Abstract

Commitment to a new cell cycle is controlled by a number of cellular signals. Mitogen-Activated Protein Kinase pathways, which transduce multiple extracellular cues, have been shown to be interconnected with the cell cycle. Using budding yeast as a model system, we have quantified in live single cells the interplay between the MAPK regulating the mating and the Cyclin-Dependent Kinase controlling cell cycle progression. Four patterns of MAPK activity dynamics could be identified by clustering cells based on their CDK activity, denoting the tight relationship between these two cellular signals. Indeed, inhibiting the CDK activity provides a direct control over the MAPK activity. Conversely, regulating the MAPK activity allows to modulate the number of cells that will enter the cell cycle. During mating, we have verified that the interplay between CDK and MAPK activities allows cells to select their fate, preventing them to be stuck in an undesirable cellular program.

Keywords

MAPK signaling, cell cycle, yeast mating, single cell analysis, fluorescent biosensors

Introduction

Cells have developed complex signal transduction pathways to respond to changes in their environment. Plasma membrane sensors detect extracellular stimuli and relay this information inside the cell via signaling cascades. These protein networks can integrate multiple information to launch the appropriate cellular response. For instance, Mitogen-Activated Protein Kinase (MAPK) pathways are central nodes in the signaling network of eukaryotic cells, because they relay extracellular cues such as growth factors or stresses[1,2]. The metabolic state, the cellular morphology or the cell cycle phase of individual cells can be integrated by the MAPK cascade to finely tune the cellular response[3-5]. However, the molecular mechanisms that allow these signal integrations are generally unknown.

The simplified settings offered by *S. cerevisiae* provide an ideal platform to study these complex mechanisms. The budding yeast MAPK network is composed of four main pathways active in haploid cells[6]. Multiple instances of signal integration have been documented in this model system: the cross-inhibition between two MAPK pathways[5], the limitation of signal transmission in low nutrient conditions[3,7] and the tight coupling between cell cycle regulation and MAPK activity[4,8-12]. In this study, we will focus on the interplay between the cell cycle and the mating pathway.

Haploid budding yeasts exist in two mating types: *MAT***a** and *MAT*$\boldsymbol{\alpha}$. They produce pheromone (respectively a-factor and α-factor) that can be sensed by a mating partner. Activation of a G-protein-coupled receptor by the pheromone leads to the activation of the MAPKs Fus3 and Kss1, via a three tiers kinase cascade recruited to the plasma membrane by the scaffold protein Ste5[13,14]. The two MAPKs initiate a transcriptional program and orchestrate the formation of a mating projection allowing the fusion of the two partners to form a diploid.

In order to guarantee that each cell that undergoes mating possesses a single copy of its genome, active Fus3 phosphorylates the Cyclin Kinase Inhibitor (CKI) Far1 which arrests the cells in G1[9,15]. In addition, during division, signaling in the mating pathway is dampened by the action of the Cyclin Dependent Kinase (CDK) Cdc28. Cdc28 is the only CDK in yeast. It associates with the different cyclins to ensure the proper progression of the cells through the cell cycle. To

inhibit the mating pathway, Cln1/2-Cdc28 complex has been shown to phosphorylate the scaffold protein Ste5, thereby preventing its recruitment to the plasma membrane[4].

Most of the knowledge on the mating-induced cell cycle arrest in G1 and the inhibition of the mating pathway during division has been obtained from population level measurements, relying on artificial synchronizations of the cell cycle using temperature sensitive mutants, chemical inhibitors or by over-expression of cyclins[4,10,15,16]. More recent studies have used single cell measurements to monitor this cross-inhibition, but focused either on MAPK activity[17,18] or on CDK activity[19].

In this study, we have developed a sensitive assay enabling to quantify in parallel MAPK and CDK activity in live single cells. Using the natural diversity present in the population, we have been able to cluster cells based on their cell cycle position and monitor their MAPK activity. We could confirm the key role of Far1 for the G1 arrest. However, our data suggest that an additional mechanism working in parallel with the Ste5 phosphorylation is required to limit signaling during division. Furthermore, we highlight the importance of the cross-inhibition between MAPK and CDK for cell-fate decision in the mating process, because the interplay between these two activities will determine whether cells induce a mating response or commit to a new cell cycle round.

Results

Quantifying MAPK activity

In order to quantify mating MAPK activity, we have developed a Synthetic Kinase Activity Relocation Sensor (SKARS). This probe was engineered by combining a specific MAPK docking site, a phosphorylatable Nuclear Localization Signal (NLS) and a Fluorescent Protein (FP)[17]. The docking site consists in the first 33 amino acids from the MAP2K Ste7, which confers specificity towards Fus3 and Kss1[20]. Under normal growth conditions, the NLS promotes the enrichment of the sensor in the nucleus. Upon activation of the MAPK, specific residues neighboring the NLS are phosphorylated leading to a decrease in the import rate of the sensor in the nucleus. The presence of the FP allows to monitor nuclear-to-cytoplasmic partitioning of the sensor as function of time (Fig 1A). Using two bright field images and a fluorescence image of

the nucleus (Hta2-tdiRFP), we are able to measure in each cell the nuclear and cytoplasmic fluorescence of the reporter[21]. The ratio of mean fluorescence intensities between these two compartments provides a dynamic measure of MAPK signaling activity in each single cell.

One experimental difficulty associated with this sensing strategy is the fact that each cell has a distinct inherent capacity to import the sensor in the nucleus. Therefore, the read-out provided for each cell includes an additional undesired component. In order to correct for this experimental variability, we introduced, in parallel to the functional sensor present in the RFP channel, a non-functional sensor in the CFP channel based on a version of the reporter that cannot bind the kinase (non-docking sensor, $Ste7_{ND}$-SKARS, Fig 1B). We define the MAPK activity as the ratio of cytoplasmic-to-nuclear fluorescence of the functional sensor over the ratio of cytoplasmic-to-nuclear fluorescence of the non-docking corrector (Supplementary Fig 1 and Methods). This metric provides a relative measure of the combined Fus3 and Kss1 activity independently of the nuclear import capacity of each cell.

We have performed time-lapse experiments where cells are stimulated with synthetic pheromone at saturating concentration (1000nM α-factor) directly under the microscope. The dynamics of activation of the mating pathway in single cells can be quantified (Fig 1C). In comparison with a signaling dead mutant (*ste5*Δ), we observe a clear increase in the median MAPK activity of the population within 5 minutes after the stimulus. However, the few single cell traces plotted in this figure display strikingly different dynamic behaviors, demonstrating well the large heterogeneity in the signaling capacity of individual cells.

Monitoring CDK activity

Because it has been established for a long time that the cell cycle can influence mating signaling competence, we decided to monitor in the same cells both MAPK and CDK activities. Fluorescently tagged Whi5 has been used in many studies as an endogenous relocation probe for G1 state[22,23]. Whi5 is enriched in the nucleus of the cells in G1 to repress the expression of specific cell cycle genes. Phosphorylation by the Cln3-CDK complex relieves this repression by promoting the nuclear export of Whi5[24,25] (Fig 1D and E). Whi5 will only shuttle back into the nucleus as cells re-enter in G1. Thus, in addition to the SKARS and its corrector, we tagged Whi5 with mCitrine and measured the cytoplasmic to nuclear fluorescence intensity in the YFP

channel as a proxy for CDK activity (Fig 1F). In a two-hour time-lapse movie, we collected single cell traces that displayed a transient nuclear accumulation of Whi5. The rapid accumulation of Whi5 in the nucleus, which corresponds to the sharp decrease in CDK activity occurring at the onset of G1, was used to synchronize computationally the single cell traces (Fig 1F and Supplementary Fig 2). Alignment of the single cell responses reveals two additional CDK activity drops taking place roughly 90 minutes before or after the central trough. This timing matches the expected cell cycle length in these conditions[26]. To sum up, this reporter strain allows us to monitor in parallel CDK and mating MAPK activities in single cells, thereby providing an assay to disentangle their interactions.

Cell cycle stage clustering

In a naturally cycling population of budding yeast cells, all cell cycle stages are represented at a given time point. Therefore, when this population is stimulated with α-factor, in a single experiment, we can observe the entire diversity of responses present in the population generated by this extrinsic variability. In a typical time-lapse experiment of 45 minutes, cells are imaged every 3 min and the pheromone is added before the third time point. From such a microscopy dataset, several hundreds of single cells are tracked and pass a quality control. Note that unless stated otherwise, all following experiments with exogenous pheromone stimulations are performed in a *bar1*Δ background, to maintain a constant extracellular concentration of α-factor in the medium surrounding the cells.

The single cell traces are clustered based on their CDK activity pattern (see Methods). The first cluster consists of cells with low CDK activity throughout the time-lapse (*G1*, 20% of the population). These *G1* cells are MAPK signaling competent and display a strong and sustained response of the SKARS upon addition of pheromone (Fig 2A). A second cluster is made of cells with a high and constant CDK activity during the 45 minutes of the time-lapse (*Out-of-G1*, 35%). Previous reports have shown, by over-expression of cyclins, that the activity of the CDK can abolish or strongly reduce the activity of the mating pathway[8,10]. Under physiological conditions, our data show that dividing cells are none-the-less able to activate the MAPK pathway, but only weakly compared to the *G1* cells.

In addition, our dynamic measurements can reveal novel signaling patterns by focusing our analysis on cells that transition between these two signaling competent and incompetent states (*G1* and *Out-of-G1*, respectively). A third cluster was thus defined with cells that start with a low CDK activity and end with high CDK activity. These cells are thus exiting G1 and enter S-phase at some point during the time-lapse (*G1-exit* 11%, Fig 2C). Interestingly, these cells respond strongly to the pheromone stimulus, but display a transient MAPK activation behavior. When pheromone is added, the mating pathway is first rapidly activated. However, when the CDK activity builds up in the cell, an inhibition of the MAPK pathway sets in leading to a return of the MAPK activity to a low level roughly 15 min after the stimulus.

The fourth cluster consists in cells that enter in G1 during the time-lapse (*G1-entry*, 31%). These cells start with high CDK activity and end the time-lapse with low CDK activity. This transition can happen at any time-point during the experiment. The median MAPK activity in this sub-population increases gradually with time, while the individual traces display sharp transitions from a low signaling to a high-signaling state (Supplementary Fig. 3A). Using the Whi5 reporter, the single cell traces were temporally aligned based on the time of G1 entry. As a result, a synchronous increase in MAPK activity is observed when CDK activity stabilizes to low values, corresponding to the G1-phase (Fig 2D and Supplementary Fig 3B). Finally, a fifth cluster was identified with cells that cycle briefly in G1 during the time-lapse (*Through-G1*, 3%). No specific behavior in MAPK activity was observed in these cells even when traces are aligned relative to the time of G1 entry (Supplementary Fig 4).

Figure 2E compares the different types of signaling behaviors observed in the four main cell cycle clusters. The MAPK signaling dynamics measured for each one of these groups is different from the global response of the population. This population response can be roughly decomposed in three main features: a step response, a small overshoot and a ramp increase. This global MAPK activity behavior has been observed multiple times with different techniques[5,17,18,27,28]. Our cell cycle clustering allows to understand the origin of this behavior by attributing it to different sub-populations (Fig 2F). *G1*-cells, which are signaling competent, display a step-like activation of the MAPKs. The graded increase in signal is generated by the asynchronous entry of cells in G1, which become signaling competent at various times. Whereas the overshoot is caused by the transient MAPK activity observed in the *G1-exit* cells. Taken together, these data

demonstrate that in different parts of the cell cycle, different types of MAPK response are monitored. As previously shown, high CDK activity limits the signaling capacity in the mating pathway. Our dynamic measurements prove that the CDK activity status is translated within a few minutes on the MAPK signaling capacity, implying a very direct link between these cellular processes.

Pheromone dose response

In order to test how the MAPK signaling behavior changes as function of input strength, time-lapse movies were recorded with various concentrations of pheromone. The same cell cycle clustering approach was used for all the dataset. Overall, the four major sub-populations display the expected MAPK dynamic behaviors. The main difference lies in the amplitude of the MAPK activity, which decreases with lower pheromone concentrations (Fig 3A-D). Smaller changes can also be observed. In the G1-phase, a sustained MAPK activity is observed at high doses of pheromone, while the signaling activity declines at lower α-factor doses (Fig 3A). This behavior suggests an interplay between positive and negative feedback loops. Multiple regulatory mechanisms have been identified in the mating pathway[27,29-31]. None-the-less, it remains difficult to estimate their relative influence on the signaling outcome. Our data demonstrate that at low α-factor concentrations, negative feedbacks are prevalent and contribute to the deactivation of the pathway. At high pheromone concentrations, however, the positive feedback stabilizes the system in a high activity state for a long time. Similar experiments were performed in *BAR1*+ cells, where the presence of the pheromone protease adds another layer of regulation to the system and leads to a faster decline in signaling activity at all concentrations but the highest one (Supplementary Fig 5).

Untreated cells (0nM α-factor) display a flat response in all cell cycle clusters except in *G1-entry*, where the basal activity of the pathway transiently drops when cells transition from M-phase into G1 (Fig 3D and Supplementary Fig 1D-F). We hypothesize that this behavior is due to the activity of the Cdc14 phosphatase during mitotic exit[32,33], which will transiently dephosphorylate the phospho-serines present in the vicinity of the NLS on the sensor. This behavior is absent in signaling dead cells (Supplementary Fig 1A-C) and is not happening to the

non-functional sensor because in both cases the NLS remains unphosphorylated and therefore insensitive to the action of the Cdc14 phosphatase.

It is well-established that treatment with pheromone prevents cells from entering a new cell cycle round[34], therefore one expect a difference in the proportion of G1 cells at the end of the experiment between α-factor treated and mock treated cells (Fig 3E). Interestingly, we noticed a gradual increase in the fraction of cells retained in G1 as function of pheromone concentration. If we focus on the population of cells starting in G1 (*G1* and *G1-exit* clusters, which roughly represent one third of the population), in the untreated situation 20% will exit G1, while 9% remain in G1 for the entire time-lapse. This proportion gradually increases to reach 20% of cells that remain in G1 at 1000nM versus 10% that can still escape G1 arrest. A similar behavior is observed for cells that are dividing at the onset of the time-lapse (*Out-of-G1* and *G1-entry*). The proportion of the cells that enter and stay in G1 (*G1-entry*) evolves from 12% to 30% as pheromone concentration increases. Thus, the larger MAPK activity measured at high concentrations promotes a larger accumulation of cells in G1 at the end of the time-lapse movie. These experiments illustrate clearly the fact that the level of MAPK activity influences the ability of the cells to initiate division.

START as a signal integration point

The START event in the cell cycle has been operationally defined as the time when cells become insensitive to a pheromone stimulus and are committed to a new cell cycle round[34]. Multiple cellular events are coordinated around this decision point. Activity of the late-G1 cyclin Cln3 increases. It triggers the exit of Whi5 out of the nucleus, thereby allowing the transcription of Cln1 and Cln2. These two cyclins will in turn drive the transcription of downstream S-phase genes[24,25,35]. We have shown that the number of cells that are blocked in G1 or commit to a new cell cycle round is dependent on the pheromone concentration and thus on the MAPK activity. In parallel, we observed that the CDK activity, estimated from the Whi5 nuclear enrichment levels, gradually increases for cells that commit to a new cell cycle round (*G1-exit* cluster, Fig 4A-D). At low pheromone concentration, cells can often override the mating signal and enter the cell cycle. However, at high concentration of α-factor only cells that have already reached a sufficient CDK activity will be able to counterbalance the mating signal, because the CDK

manages to push the cell in a new division round. Interestingly, at high α-factor concentrations, we observe a few traces where CDK activity seems to be only transiently increasing and where we suspect that the addition of the pheromone inhibited the progression of the cell cycle (Fig 4E). Taken together these results comfort the idea that START is a signal integration point where the cells balance the relative MAPK and CDK activities to determine their fate: division or mating.

Hence, the cross-inhibition between the MAPK and CDK plays a central role in the decision to mate or divide. The molecular mechanisms regulating the interplay between mating and cell cycle have been extensively studied. Phosphorylation and expression of Far1 upon α-factor stimulus inhibit the Cln1/2-Cdc28 complex to prevent cell cycle progression into S-phase[9,36,37]. Deletion of FAR1, does not affect the MAPK signaling activity of *G1* nor of *Out-of-G1* cells (Supplementary Fig 6A). However, the fraction of cells found in G1 at the end of the time-lapse experiment is increasing from 25% to 50% for WT cells when changing the pheromone concentration to 1μM, while it remains below 30% in *far1*Δ (Supplementary Fig 6B). These results confirm the important role played by Far1 in the G1-arrest during the mating response.

Modulating Cdc28 activity

We have shown above that the efficiency of the cell cycle arrest depends on the level of MAPK activity. We next want to verify how different levels of CDK activity influence the MAPK signal transduction. In yeast, a single Cyclin Dependent Kinase, Cdc28, associates with the different cyclins throughout the cell cycle to orchestrate the division of the cell. While Cdc28 is an essential protein, it is none-the-less possible to acutely inhibit its kinase activity by using an analogue sensitive allele (*cdc28-as*,[38]). The inhibitor NAPP1 was added to the cells 6 minutes after the pheromone stimulus. Upon NAPP1 treatment, *Out-of-G1* cells show a rapid relocation of Whi5 in the nucleus, attesting the fact that CDK activity is blocked. In parallel, the MAPK activity that is low during division increases to a level comparable to the one observed in cells stimulated in G1 (Fig 5A).

Additionally, this experiment allows to verify that the transient MAPK activation observed in the *G1-exit* cluster is shaped by the rising CDK activity. Cells with an increasing CDK activity after pheromone stimulus were clustered. In the DMSO control experiment, this sub-population

displays the expected fast activation of the MAPK upon α-factor addition followed by a decay to basal activity as CDK activity rises. In the inhibitor treated cells, the MAPK activity decay is blocked upon NAPP1 addition and the MAPK signal rises to reach full activity (Fig 5B). These experiments demonstrate that the activity of Cdc28 directly and quickly regulates the level of MAPK activity allowed in the cell.

In order to better characterize the relationship between CDK and MAPK activities, we performed a set of experiments where the CDK of cells in division was inhibited to various extents using a range of NAPP1 concentrations (Fig 5C and Supplementary Fig 7). Twenty minutes after the addition of the inhibitor, the pheromone stimulus was applied to stimulate the MAPK. As expected, there is a clear inverse correlation between the MAPK and CDK activities. A Hill function was fitted on the data points representing the CDK activity versus the inverse MAPK activity. Using this simple relationship, we can predict the expected MAPK activity based on the measured CDK levels for cells that start out of G1 or cells that exit G1 (Fig 5D and E). In both cases, there is a good agreement between the measured and the predicted MAPK activity curves. However, this simple model cannot account for the behavior observed upon G1 entry. Based on the CDK activity level, the model predicts a rise in MAPK activity 10 minutes earlier than what is observed experimentally. While the small temporal difference between predicted and measured MAPK activity in Figure 5D and E can be rationalized by a small temporal delay required for the CDK to phosphorylate its target, the longer delay observed for the *G1-entry* cells argues in favor of a more complex regulatory mechanism present at this transition phase before signaling competence is reestablished in G1 cells.

Ste5 inhibition by the CDK

Confronting experiments and model predictions allowed us to verify the tight relationship between MAPK and CDK activities. Presently, the described mechanism of inhibition of the mating pathway by the CDK consists in the direct phosphorylation of the scaffold Ste5 by the Cln1/2-Cdc2 complex [4]. Eight consensus phosphorylation sites in the vicinity of a plasma membrane binding domain (PM) in Ste5 are targeted by the CDK to alter the charge of this peptide. This phosphorylation prevents the association of Ste5 to the membrane, thereby blocking the signal flow in the pathway. In *ste5*Δ cells, we reintroduced three different alleles of

Ste5 at the endogenous locus: the WT copy, the $Ste5_{8A}$ mutant (where all putative phosphorylatable residues were mutated to alanine[4]) or a $Ste5_{ND}$ (where the docking motif of Cln1/2 on Ste5 has been mutated[39]) (Fig 6A). The wild-type *STE5* behaved similarly to the WT parental strain, demonstrating that the complementation strategy is working. As expected, signaling activity in *G1* cells was not influenced by either mutation in Ste5 because the CDK is inactive. In the *Out-of-G1* cluster, we observed a small but significant increase in MAPK signaling activity for the two Ste5 mutants compared to the WT allele (Fig 6B and C). Because we don't recover the full MAPK signaling activity, our data suggest that during periods of high CDK activity, Ste5 phosphorylation is not the sole mechanism present that limits the signal transduction in the mating pathway. Inhibiting *cdc28-as* in $Ste5_{ND}$ cells allows to recover full MAPK activity (Fig 6D). In addition, the delay in MAPK signaling activity in the *G1-entry* cells is also present in the $Ste5_{ND}$ mutants (Fig 6E, compare to Fig. 5F).

The discrepancy between our findings and the previous data[4], which showed that the introduction of a $Ste5_{8A}$ was sufficient to abrogate all cell cycle regulation of the mating pathway is puzzling. However, the two studies differ on many aspects. Pryciak's group used primarily an over-expression of Cln2 to simulate S-phase conditions and quantified the induction of a gene expression reporter (p*FUS1*-lacZ) when cells were subjected to saturating levels of pheromone[4]. Our experiments are performed in naturally cycling cells, using clustering to differentiate the cell cycle phases. In addition, we quantify the kinase activity of Fus3 and Kss1 for a wide range of α-factor concentrations. The discrepancy could be explained by the levels at which the MAPK signal is evaluated: at the transcriptional output level in the previous study; at the kinase activity level in our study. Therefore, in a strain bearing the Whi5-mCitrine, Hta2-tdiRFP and the $Ste5_{WT}$ or $Ste5_{8A}$, we introduced a dynamic single cell expression reporter under the control of a strongly inducible mating promoter (p*AGA1*-dPSTR^{R} [40,41] Supplementary Fig 8). For the $Ste5_{WT}$ allele, a clear difference in expression dynamics can be observed between *G1* and *Out-of-G1* cells. Interestingly, at high concentrations of pheromone (100nM), this difference is completely abolished in the $Ste5_{ND}$ mutant. However, at low concentrations (10 nM), a difference in expression dynamics can be observed as function of the cell cycle stage (Supplementary Fig 8). Taken together these data demonstrate that the CDK activity limits the signaling capacity of the mating pathway. The phosphorylation of Ste5 seems to be one of the mechanisms for this

inhibition. The additional mechanism(s) for this process remain(s) to be identified. Ste20 has been often suggested as a potential target for this regulation[42-44]. We have tested various alleles of Ste20 but did not notice any alleviation of the CDK inhibition in these strains (Supplementary Fig 9 A and B). We have also tested the influence of phosphorylation sites on Ste7 without measuring any detectable changes in signaling activity between mutants (Supplementary Fig 9 C and D).

To summarize, START is the integration point where MAPK and CDK activities are compared to engage in a specific cellular fate. Far1 and Cdc28 are key players in this cross-inhibition of the two pathways. *far1*Δ cells cannot arrest their cell cycle at START, none-the less, a number of Far1-independent mechanisms for cell cycle arrest have been documented[45-47]. Cdc28 is solely responsible for the inhibition of the mating pathway by the cell cycle and, up to now, only a single target, Ste5, has been convincingly shown to regulate this process. Our data indicate that other mechanisms, that remain to be identified, must contribute to the repression of MAPK activity in dividing cells.

MAPK activity in mating

After studying the response of cells stimulated by exogenous pheromone, we next wanted to understand how the cell cycle and the mating pathway were regulated during mating and how this cross-inhibition allowed an efficient cell-fate selection in these physiological conditions. In order to achieve this, we have imaged the *MAT***a** cells bearing the SKARS, the corrector and the Whi5 marker in presence of a *MAT*$\boldsymbol{\alpha}$ partner expressing constitutively a cytosolic CFP at high levels. In Figure 7A, thumbnails of such an experiment are displayed. The fusion events (arrow heads) can be detected by observing a sudden increase in CFP signal in the *MAT***a** cells. In the frame preceding the two fusions events displayed in Figure 7A, we observe that the *MAT***a** cells of interest are in G1 (nuclear Whi5) and display a high MAPK activity (nuclear depletion of the SKARS).

The dynamic measurements of the mating process allow us to monitor how cells reach this state. Using our automated image analysis pipeline, we have detected on the order of hundred fusion events and curated them manually to remove any artifacts due to a mis-segmentation of the cells. The single cell traces of these events have been computationally aligned relative to the fusion

time. Time zero corresponds to the last frame before the increase in CFP intensity, because it is the last time point where MAPK activity can be reliably quantified. Compared to the median value of cells imaged in the same conditions, but in absence of mating partner, a gradual increase in MAPK activity starts 40 to 60 minutes prior to fusion (Fig 7B). In parallel, we observe that the median CDK activity is low for all time-points. However, the 75 percentile stabilizes to a low value 40 minutes prior to fusion, denoting that a fraction of the population enters in G1 within the hour preceding the fusion.

Interestingly, the Ste5 mutant alleles ($Ste5_{8A}$ or $Ste5_{ND}$) display a very similar behavior during the mating process. The MAPK activity rises 40 min before fusion, a time when a large fraction of the population has stabilized in G1 state (Figure 7C). In the Ste5-wt and the two Ste5 mutant alleles, we monitored when cells entered G1 prior to the fusion time. Seventy-five minutes prior to fusion, more than two thirds of the population have already entered G1 and will remain in this state until fusion occurs (Figure 7D). Thirty minutes before fusion, more than 95% of the cells are found in G1. Visual inspection of the few cells that fused out of G1, confirmed a G1 state which was not picked up by the automated analysis of the single cell traces. To conclude, while the $Ste5_{8A}$ and $Ste5_{ND}$ mutants are able to hyperactivate the mating transcriptional response in S-phase, this property is not sufficient to bypass the requirement to fuse in G1-state. This is an additional evidence that suggests that an alternative mechanism is in place that limits signaling in the mating pathway during phases of high CDK activity.

From the analysis of these fusion events, it becomes clear that the enrichment in G1 state prior to fusion is made in cells that experience a low level of MAPK activity, or, in other words, when cells are surrounded by a low concentration of mating pheromone. In the exogenous stimulation experiments, we have shown that at low pheromone concentrations, a fraction of the cells do not commit to the mating response and keep proliferating. We wondered whether in the mating mixtures, non-fusing cells were influenced by the presence of the mating partners. To achieve this, we monitored the CDK activity in cells that were cycling through G1. Interestingly, we observe that the G1 state is slightly prolonged and that the CDK activity remains lower in cells in mating mixtures compared to the same cells imaged alone (Figure 7E and F). We believe that these differences are due to a weak activation of the mating pathway (Supplementary Fig 10). *ste5*Δ cells imaged in presence of a mating partner display a fast cycling through G1 compared to

the WT cells because they remain insensitive to the presence of the partners. In this background, the deletion of the scaffold Ste5 leads to an absence of activity of the MAPK Fus3 and Kss1 which cannot counteract the rise of the CDK activity at START.

Discussion

We have verified with exogenous stimulation experiments performed with various concentrations of pheromone that START is a central integration point where cells compare the relative levels of MAPK and CDK activities to decide on their cellular fate: proliferation or mating. It remains to be precisely determined which molecular mechanisms control this decision. On the CDK side, Cdc28 kinase activity is directly regulating the signal flow in the MAPK pathway. Blocking Cdc28 activity relieves this inhibition allowing to recover full MAPK activity, within minutes after addition of the chemical inhibitor (Figure 5). This suggests a very direct mechanism of action on the mating pathway. The primary candidate for this process has been Ste5. However, our quantitative measurements speak for an additional mechanism. Other potential candidate targets of Cdc28 could be the G-protein and the receptor or other proteins in the MAPK signal transduction cascades.

On the MAPK side, our data agree with the numerous previous studies that demonstrated that the MAPK activity controls the CDK via the protein Far1[9,15]. The mating pathway regulates both the level of Far1 and its phosphorylation status. What remains to be understood is how each one of these changes influence the decision made by the cell. If we could measure those quantities precisely in individual cells, would it be sufficient to predict the fate of individual cells?

The experiments performed with mating mixtures also illustrate that the interplay between the CDK and the MAPK are central elements in the cell-fate choice taken by the cells. In a mating mixture, every time a cell enters in G1, it will activate the mating pathway to a low level. This low MAPK activity is sufficient to slow down the progression of G1. If a partner is present in the vicinity, the mating pathway activity will increase further, lowering the chance that the CDK activity rises sufficiently to promote a new cell cycle round. However, at any time point during this sensing phase, a decrease in MAPK activity can result in a commitment to a new cell cycle round. These cell fate choices are taking place at low levels of MAPK signaling activity, where

we have shown with exogenous pheromone stimulation, that the CDK frequently overrides the MAPK arrest. If a cell remains long enough in the mating program, MAPK signaling activity will slowly rise as the coordinated secretion of mating pheromone by the two partners will promote the shmooing and ultimately the fusion of the two haploid cells.

MAPK signaling and the cell cycle are cellular processes highly conserved throughout eukaryotes. The homolog of Fus3 in mammalian cells is ERK. ERK is probably best known for its implication in cell growth and division in somatic cells[48] and hyperactivating mutation in the ERK pathway are found in numerous cancers[49]. However, the ERK pathway can also inhibit cell cycle progression. One well-known example is the stimulation of PC-12 cells with NGF, which results in a prolonged activation of ERK, promoting a cell cycle arrest and a differentiation into neuronal cells[50,51]. More generally, during development MAPK pathways play a central role in the commitment of cells into specific lineage and this is often performed in tight correlation with the cell cycle[52].

Materials and Methods

Strains and plasmids

Yeast strains and plasmids are listed in Supplementary Tables 1 and 2. SKARS plasmids were constructed by cloning the different sensors from Durandau et al[17] into a pSIV vector backbone[53]. The sensor and the corrector were assembled by cloning the $STE7_{1\text{-}33}$ *-NLS-NLS-mCherry* or the $STE7_{ND}$*-NLS-NLS-CFP* (HindIII-KpnI) sequences downstream the p*RPS6B* promoter into the pSIV-URA (SacI-KpnI). The plasmid pED141 containing both sensor and corrector was obtained by cloning the p*RPS6B* -$STE7_{ND}$ *-NLS-NLS-CFP* into the second MCS of pED92 (AatII-SphI). Plasmids were transformed in yeast of W303 background expressing the Hta2-iRFP (yED136) or the Hta2-tdiRFP (yED152). Whi5 was tagged with mCitrine using pGTT-mCitrine plasmid[53].

Genomic deletions were constructed in cells bearing the sensors using KAN or NAT resistance cassettes[54,55]. Plasmids containing the coding sequence of Ste5, Ste20 and Ste7 were obtained by amplification of a chromosome fragment spanning from -100bp (into the promoter) to the end of the ORF and cloned using PacI-NheI sites into the pGTH-CFP (replacing the fluorescent protein). Mutated variants were then obtained by replacing a portion of the plasmid DNA coding sequence by a synthetic double-stranded DNA fragment bearing the desired mutations. Plasmids were integrated into the genome of yeast by replacing the NAT or KAN cassettes used to delete the native gene using homology regions in the promoter of the gene and in the TEF terminator of the deletion cassette, which is also present on the pGTH vector.

Sample preparation

The cells were grown to saturation in overnight cultures at 30°C in synthetic medium (YNB: CYN3801, CSM: DCS0031, ForMedium). They were diluted in the morning to OD_{600}=0.05 and grown for at least four hours before starting the experiments. For experiments in wells, 96-well plates (MGB096-1-2LG, Matrical Bioscience) were coated with a filtered solution of Concanavalin A (0.5 mg/ml, 17-0450-01, GE Healthcare) for 30min, rinsed with H_2O, and dried for at least 2 hours. Before the experiment, the cultures were diluted to an OD_{600} of 0.05, and briefly sonicated. A volume of 200µl of culture was loaded into each well. Cells were left settling 30-45 minutes before imaging. To stimulate the cells, 100µl of inducing solution was added to the wells. For α-factor stimulation, final concentration is indicated into the figure legend. To inhibit the *cdc28-as*, a 25mM stock solution of NAPP1 (A603004, Toronto Research Chemical) in DMSO was diluted in SD-medium and added to the wells. The final working concentration is indicated in the figure legend. For control experiments, cells were treated with DMSO 0.16 % in SD-full.

For mating assay experiments, log phase cultures of *MAT***a** and *MAT*$\boldsymbol{\alpha}$ (ySP694) were diluted to OD 0.1 in 500µl SD-full. Cells were spun down for 2min at 3000rpm. The supernatant was removed from the cultures and *MAT*$\boldsymbol{\alpha}$ cells were resuspended in 10µl of SD-full. These 10µl were then used to resuspend the *MAT***a** cells. 1µl of this mating mixture was placed on an agar pad. The pad was then placed upside down into the well of a 96-well plate. To prepare the pad, a 2% agarose mixture in SD-full was heated for 5 min at 95°. 150µl liquid was placed in a home-

made aluminum frame. After cooling down, the 7 mm square pad was gently extracted from the frame. Typically, 6 to 8 mating pads were prepared and imaged in parallel.

Microscopy

Images were acquired with a fully automated inverted epi-fluorescence microscope (Ti-Eclipse, Nikon), controlled by Micromanager software[56] and placed in an incubation chamber set at 30 °C, with a 40X oil objective and appropriate excitation and emission filters. The excitation was provided by a solid-state light source (SpectraX, Lumencor). The images were recorded with a sCMOS camera (Flash4.0, Hamamatsu). A motorized XY-stage allowed recording multiple fields at every time points. Cy5p5 (200ms), CFP (100ms), RFP (100ms), YFP (300ms) and two brightfield (10ms) images were recorded at time intervals of 3 or 5 minutes (Fig 7).

Data analysis

Time-lapse movies were analyzed with the YeastQuant platform[21]. The cell nuclei were segmented by thresholding from Cy5p5 images. The contour of the cell around each identified nucleus was detected using both brightfield images. The cytoplasm object was obtained by removing the nucleus object expanded by two pixels from the cell object. The nuclei were tracked across all the frames of the movie. Multiple features of each object were quantified. Note that for mating pad experiments, the *MAT*α cells were not segmented as they do not express the Hta2-iRFP. Dedicated scripts were written in Matlab R2016b (The Mathworks) to further analyze the data. Except for Figure 7, only cells tracked from the beginning to the end of the movie were taken into consideration. In addition, a quality control was applied on each trace and only the traces with low variability in nuclear and cell area, and Cy5p5 nuclear fluorescence were kept for further analysis. On average, 65% of the cells tracked from the beginning to the end of the time-lapse passed the quality control.

For each cell, the average nuclear intensity in the fluorescent channel corresponding to the SKARS, the Corrector and Whi5-mCitrine were divided by the average intensity in the cytoplasm for every time point (ratio N/C). To quantify the MAPK activity, the Adjusted ratio for each individual cell was obtained by dividing the ratio N/C of the Corrector by the ratio N/C of the SKARS. The CDK activity of each cell was defined as the inverse of the Whi5-mCitrine N/C

ratio. The initial CDK activity was defined as the average of three time-points before the stimulus (3-6 minutes before α-factor stimulus). For the *cdc28-as* NAPP1 dose response experiment, initial/final MAPK and CDK activities were defined as the average of the time-points pre/post α-factor addition (Pre-stimulus: -6 to -3 minutes prior pheromone addition. Post-stimulus: from 10 min after pheromone addition). All these quantities are unitless numbers, since they are ratios between fluorescence intensities obtained from the microscope camera. We used the symbol [–] to represent this lack of units.

Modeling of CDK-dependent MAPK activity

From the NAPPI dose response experiment presented in Supplementary Fig 7, we extracted the MAPK activity and the CDK activity either prior ($MAPK_{Ini}$, CDK_{Ini}) or after stimulation with α-factor ($MAPK_{Final}$, CDK_{Final}) for each individual cell. The median of these parameters were calculated for each experiment including all replicates. We plotted the data using a scatter plot showing the 1/MAPK parameters versus the CDK parameters (Fig 5C, Supplementary Fig 7E). We then used the fit function of Matlab to fit our data. For the scatter plot of $1/MAPK_{Final}$ against CDK_{Final} we obtained the best fit using a Hill equation. For the scatter plot of $MAPK_{Ini}$ against CDK_{Ini} we obtained the best fit using a linear equation. These two equations were then used to estimate the MAPK activity ($MAPK_{fit}$) from the dynamic CDK activity data. The estimated $MAPK_{fit}$ activity prior pheromone addition was defined as:

$$\frac{1}{MAPK_{fit_{Ini}}} = A \cdot CDK_{Ini} + B$$

The best fit was obtained with A = 0.3 and B = 0.98.

Under stimulating condition:

$$\frac{1}{MAPK_{fit_{Final}}} = \frac{{CDK_{Final}}^{n}}{{CDK_{Final}}^{n} + C} + D$$

The best fit provided the coefficients C = 0.7, D = 0.6 and n = 6.

Dynamic single cell MAPK and $MAPK_{fit}$ values are then plotted against the time relative to pheromone addition (Fig 5D-E) or relative to G1 entry (Fig 5F) for comparison. Note that for the *G1-entry* cluster, only the values after pheromone stimulation were considered.

CDK activity-based clustering and synchronization

When plotting a histogram using the Whi5 ratio N/C (Nuclear intensity over Cytoplamsic intensity) of all cells at all time-points, we identified two populations. To properly distinguish between ratios corresponding to nuclear Whi5 versus ratios corresponding to cytoplasmic Whi5, we first separated ratio values using a fixed threshold (threshold=2). However, this value overestimated the limit of what could be considered as nuclear Whi5. We then identified cells with ratios below this threshold at all time points and replotted a histogram of all Whi5 ratio N/C values from this sub-population. This method enables to enrich the sample with low N/C ratio. This second histogram presented a clearer overview of the values corresponding to cytoplasmic Whi5. We then calculated the derivative of the histogram and identified the position of fifth-lowest derivative value . The corresponding Whi5 ratio N/C was used as a final threshold to separate nuclear to cytoplasmic Whi5 values. This procedure enables to correct for slight differences between experiments mostly due to the chosen experimental settings (96 well-plate or pad experiments). Globally, the procedure adjusted the threshold between 2 and 1.7. If the Whi5 ratio N/C was above the threshold, corresponding to a low CDK activity value (C/N) and thus the cell was considered in G1. On the opposite, values below the threshold indicates that the cell was *Out-of-G1*. *G1* cells sub-population was defined by single cell traces which remained above the threshold for the entire duration of the time-lapse. Conversely, *Out-of-G1* cells cluster was defined by traces that stay below this threshold. The other single cell traces are scanned for G1-entry and G1-exit events. If a pattern of two values below the threshold followed by two values above the threshold was found, we considered that the cell belonged to the *G1-entry* cluster. The same strategy was used to identify the *G1-exit* sub-population, using a pattern of two values above the threshold followed by two values below the threshold. Cells in the *G1-entry* cluster were defined as having a single event of G1-entry. Cells in the *G1-exit* cluster were selected as having only one event of G1-exit. Finally, the *Through-G1* cluster is made of cells that display a G1-entry event followed by G1-exit event. Because the duration of the time-lapse experiments is much shorter than the cell cycle of the yeast (45 min vs 90 min), we considered

that the number of events cannot exceed two. Cells which do not follow this criterion were rejected from the analysis. Depending on the experiment, we rejected a maximum of 5% of the total population. The position of the G1-entry was used to create new time vectors for synchronization of the *G1-entry* and the *Through-G1* single cells traces. We extracted the individual time vector for each cell and subtracted the time at which the G1-entry event occured.

Detection of fusion events in mating assays

MATα cells express the CFP fluorescent protein under the control of a strong promoter. When *MAT***a** and *MAT*α cells fuse the CFP from the *MAT*α cell diffuses into the partner leading to a rise of the fluorescence into the segmented *MAT***a**. Fusing *MAT***a** cells were first detected bioinformatically by identifying a sudden increase of the CFP intensity in the nucleus object. We chose the nucleus object rather than the whole cell to avoid that mis-segmentation triggers a misleading increase in CFP intensity not linked to a fusion event. Fusion event time was defined as the time point at which the difference in the CFP nuclear signal between two consecutive time-points exceed 200, while remaining below 700. Traces of fusing cells were selected as they contain a single detected fusion event. We filtered out cells with aberrant absolute and derivative nuclear CFP fluorescence signal or tracked for less than 15 min prior or after the fusion time. CFP images corresponding to selected cells were checked manually to reject false positives that could not be detected during the bioinformatics analysis. The position of the fusion event into the time vectors of individual fusing cells was used as a time reference to align temporally the MAPK activity and CDK (Figure 7).

Acknowledgments

We thank all members of the Pelet and Martin labs for helpful discussions and comments on the manuscripts, Marta Schmitt and Clémence Varidel for technical assistance. This study was supported by Swiss National Science Foundation grants (PP00P3_139121) and the University of Lausanne.

Author contributions

ED and SP conceived and study and wrote the manuscript. ED constructed the strains and performed the experiments with exogenous stimulation of pheromone. SP performed the mating assays experiments. ED analyzed the single cell data.
The authors declare no competing financial interests

Figure Legends

Figure 1: Dynamic MAPK and CDK activity measurements in live single cells.

A. Schematic representation of the Synthetic Kinase Activity Relocation Sensor (SKARS).

B. Epi-fluorescence microscopy images of WT cells expressing a Hta2-tdiRFP (nucleus), a $Ste7_{DS}$-SKARS-mCherry (MAPK activity sensor), a $Ste7_{ND}$-SKARS-CFP (Corrector), and a Whi5-mCitrine (CDK activity). Cells were stimulated with 1μM α-factor at time 0.

C. MAPK activity was quantified from time-lapse movies acquired with a WT strain (red, Nc = 191) and a mating signaling dead mutant (*ste5Δ*, blue, Nc = 437) (See Methods and Supplementary Fig 1). For all similar graphs, the solid line represents the median of the population, the shaded area delimits the 25 and 75 percentiles of the population. Dashed lines display the response of a few single cells. Nc represents the number of single cell traces analyzed.

D. Schematic representation of the CDK activity sensor (Whi5-mCitrine).

E. Microscopy images of the same strain presented in B. The thumbnails are extracted from a 120 min time-lapse movie of unstimulated cells dividing under normal growth conditions.

F. CDK activity reported as function of time relative to G1. Single cell traces that exhibit at least one trough of CDK activity were selected (Nc = 70). The traces were synchronized relative to the time at which the CDK activity reaches its minimum value (see Supplementary Fig 2).

Figure 2: Dynamics of MAPK activity in different cell cycle phases.

A-D. MAPK activity was quantified for cells in an asynchronously growing culture stimulated with 1μM α-factor at time 0. 738 single cell traces were clustered by comparing the CDK activity prior and after stimulation (see Methods). *G1* cells (A, Nc =143) retain a low CDK activity throughout the time-lapse, while *Out-of-G1* cells (B, Nc =256) maintain a high CDK activity. *G1-exit* cells (C, Nc =76) start with low and finish with high CDK activity. Conversely,

G1-entry cells (D, Nc =249) start with high and finish with low CDK activity. In this sub-population, the traces are aligned relative to the time of G1-entry. The median (solid line) MAPK activity (red) and CDK activity (green) and the 25-75 percentiles (shaded area) of each sub-population are plotted.

E. Summary of the various dynamic MAPK activities observed in the four main cell cycle clusters. Each line corresponds to the mean of the medians of 5 biological replicates. Error bars represent the standard deviations of the medians. The percentages in the legend indicate the relative proportion of each cluster in the population.

F. The dynamic behaviors of each cluster were summed to each other taking into account their prevalence in the population. The different features of the MAPK activity behavior at the population level can be explained by the contributions from each cell cycle cluster.

Figure 3: Commitment to cell cycle is pheromone dose-dependent.

A-D. Pheromone dose-dependent dynamic MAPK activity in different phases of the cell cycle. Experiments and clustering analysis were performed as in Figure 2. Different α-factor concentrations were used to stimulate cells. Median MAPK activity from at least five replicates were averaged for each curve. The error bars represent the standard deviations between the replicates.

E. Fractions of cells in each sub-population as function of the pheromone concentration. The prevalence of each cluster is calculated from the means of at least three replicates.

Figure 4: Level of MAPK activity at START controls cell cycle commitment.

A-C. Dynamic CDK activity of cells exiting G1 at various pheromone concentrations. Single cell traces (dashed lines) and the median of the sub-population (solid line) are presented in each graph. Note the decreased variability in CDK activity patterns as pheromone concentration increases.

D. Initial CDK activity measured in the *G1-exit* cluster for different α-factor concentrations. The distribution of the initial CDK of *G1-exit* cells for one replicate for each concentration is presented as a boxplot. The dots correspond to the median initial CDK activity of additional replicates.

E. CDK activity of cells attempting to exit G1. The dynamic CDK activity of G1 cells from multiple 1000nM α-factor experiments were pooled. The Attempt G1-exit sub-population (red) contains cells with an initial CDK activity above 0.35. Four single cell traces from the Attempt G1-exit sub-population (dashed lines) that display a transient peak in CDK activity around the time of pheromone addition are plotted. The median CDK activity for the *G1* (blue) and *G1-exit* (green) clusters from Figure 2 are plotted for comparison.

Figure 5: Regulation of MAPK signal transduction by the CDK.

A-B. Dynamic CDK and MAPK activities after *cdc28-as* chemical inhibition. Cells expressing an analogue sensitive allele of Cdc28 (*cdc28-as*) are imaged every two minutes for 50 minutes. Cells are stimulated with 100nM α-factor at time 0. Six minutes later either NAPP1 (10 μM, solid line and shaded area) or DMSO (0.04% v/v, dashed line) is added. MAPK and CDK activities of cells starting *Out-of-G1* (mean $CDK_{t<0}$ >0.5, A, NAPP1: Nc = 448, DMSO: Nc = 381), or exiting G1 upon pheromone addition (mean $CDK_{t<0}$ <0.5 and mean $CDK_{0<t<6}$ >0.5, B, NAPPI: Nc = 39, DMSO: Nc = 16) are plotted.

C. Correlation between the inverted MAPK activity and the CDK activity for *cdc28-as* cells treated with various concentrations of NAPP1 and subsequently stimulated with a saturating concentration of pheromone (see Methods and Supplementary Fig 7). Each dot represents the median CDK activity and 1/MAPK activity from one experiment. The color indicates the concentration of NAPP1 used. The red line is a fit of these data points using a Hill function.

D. Dynamic CDK (green) and MAPK (red) activities from one replicate of the assay described in A are plotted for the sub-population of cells starting out of G1. Dynamic CDK activity from each single cell traces are used as input to predict their MAPK activities (dashed line: median $MAPK_{fit}$, Nc =186).

E-F. CDK and MAPK activities of the *G1-exit* (E) and *G1-entry* (F) sub-populations isolated from a *cdc28-as* DMSO control experiment analyzed as in Figure 2C and D. The dynamic MAPK activity of each single cell ($MAPK_{fit}$) is modeled and averaged as in panel D (E, Nc =25; F, Nc =87).

Figure 6: Dynamic MAPK activity of cells expressing non-phosphorylatable Ste5 alleles.

A. Schematic representation of the wild-type Ste5 scaffold protein structure compared to the $Ste5_{8A}$ mutant with 8 non-phosphorylatable residues in the vicinity of the plasma membrane domain and the $Ste5_{ND}$ variant with point mutations in the Cln1/2 docking motif.

B. Dynamic MAPK activity of *G1* and *Out-of-G1* cells expressing either the WT (Nc=1000 for all clusters) or the $Ste5_{ND}$ allele (Nc=415 for all clusters). Experiments and analysis were performed as in Figure 2.

C. Comparison of the MAPK response in $Ste5_{WT}$, $Ste5_{8A}$ and $Ste5_{ND}$ alleles for the *G1* and *Out-of-G1* sub-populations for various pheromone concentrations. Values are means of at least three replicates and error bars represent the standard deviations.

D. The *cdc28-as* strain expressing the $Ste5_{ND}$ is imaged and analyzed as in Figure 5A (Nc=313). Six minutes after pheromone stimulation, the Cdc28 activity is blocked by addition of NAPP1.

E. CDK and MAPK activities of the *G1-entry* sub-population expressing the $Ste5_{ND}$ allele and imaged and analyzed as in Figure 5F (Nc=99, *cdc28-as strain*, DMSO control sample).

Figure 7: CDK and MAPK cross-regulation in mating conditions

A. Microscopy time-lapse images of two fusion events between *MAT***a** cells expressing the various sensors mixed with *MAT*α strain expressing a cytoplasmic CFP. The fusion can be detected when the CFP from the *MAT*α diffuses in the *MAT***a** partner (White arrows). The indicated time is relative to the last time point preceding the second fusion event.

B-C. Dynamic MAPK and CDK activities in *MAT***a** cells undergoing fusion detected by a sharp increase in CFP intensity (blue) (See Method). MAPK (red) and CDK (green) activities of the fusing cells were synchronized relative to the last time point before the fusion occurs (). The dashed orange line and the shaded area around it correspond to the median and 25-75 percentiles (averaged across multiple timeponits) of the MAPK activity in *MAT***a** cells in absence of mating partners, but imaged in the same conditions. *MAT***a** cells express either a WT allele of Ste5 (**B.** *MAT***a**, $STE5_{WT}$ X *MAT*α *WT*, Nc=127) or a mutated version of the scaffold protein (**C.** *MAT***a**, $STE5_{8A}$ X *MAT*α *WT*, Nc=103) are crossed to WT cells.

D. Cell-cycle position of fusing cells. *MAT***a** strains expressing one of the three Ste5 alleles described in Figure 6A were crossed with the WT. The CDK activity is used to quantify the average fraction of cells in G1 at multiple time intervals prior to fusion. Each bar represents the mean of at least three replicates. Error bars correspond to the standard deviations.

E-F. Duration of the G1 phase of non-fusing cells. Non-fusing cells transiting through G1 were identified as previously (Fig 3C and Methods). **E.** The dynamic CDK activity from single cells are synchronized relative to the G1 entry and averaged as in Fig 2D (Error bars are standard deviation of at least three median replicates). **F.** The time separating the G1 entry and G1 exit is calculated from each single cell trace ($\Delta t_{exit - entry}$) and averaged. The mean $\Delta t_{exit - entry}$ from at least three replicates are plotted as boxplot.

In these mating experiments, all strains are BAR1.

References

1. Chen, R. E. & Thorner, J. Function and regulation in MAPK signaling pathways: lessons learned from the yeast Saccharomyces cerevisiae. *Biochim Biophys Acta* **1773,** 1311–1340 (2007).
2. Roux, P. P. & Blenis, J. ERK and p38 MAPK-Activated Protein Kinases: a Family of Protein Kinases with Diverse Biological Functions. *Microbiology and Molecular Biology Reviews* **68,** 320–344 (2004).
3. Clement, S. T., Dixit, G. & Dohlman, H. G. Regulation of yeast G protein signaling by the kinases that activate the AMPK homolog Snf1. *Science Signaling* **6,** ra78–ra78 (2013).
4. Strickfaden, S. C. *et al.* A mechanism for cell-cycle regulation of MAP kinase signaling in a yeast differentiation pathway. *Cell* **128,** 519–531 (2007).
5. Nagiec, M. J. & Dohlman, H. G. Checkpoints in a yeast differentiation pathway coordinate signaling during hyperosmotic stress. *PLoS Genetics* **8,** e1002437 (2012).
6. Saito, H. Regulation of cross-talk in yeast MAPK signaling pathways. *Current opinion in microbiology* **13,**

677–683 (2010).
7. Sharifian, H. *et al.* Parallel feedback loops control the basal activity of the HOG MAPK signaling cascade. *Integrative biology : quantitative biosciences from nano to macro* **7,** 412–422 (2015).
8. Oehlen, L. J. & Cross, F. R. G1 cyclins CLN1 and CLN2 repress the mating factor response pathway at Start in the yeast cell cycle. *Genes & Development* **8,** 1058–1070 (1994).
9. Peter, M. & Herskowitz, I. Direct inhibition of the yeast cyclin-dependent kinase Cdc28-Cln by Far1. *Science* **265,** 1228–1231 (1994).
10. Wassmann, K. & Ammerer, G. Overexpression of the G1-cyclin gene CLN2 represses the mating pathway in Saccharomyces cerevisiae at the level of the MEKK Ste11. *J Biol Chem* **272,** 13180–13188 (1997).
11. Escoté, X., Zapater, M., Clotet, J. & Posas, F. Hog1 mediates cell-cycle arrest in G1 phase by the dual targeting of Sic1. **6,** 997–1002 (2004).
12. Clotet, J. & Posas, F. Control of cell cycle in response to osmostress: lessons from yeast. *Meth Enzymol* **428,** 63–76 (2007).
13. Bardwell, L. A walk-through of the yeast mating pheromone response pathway. *Peptides* **26,** 339–350 (2005).
14. Atay, O. & Skotheim, J. M. Spatial and temporal signal processing and decision making by MAPK pathways. *J Cell Biol* **216,** 317–330 (2017).
15. Peter, M., Gartner, A., Horecka, J., Ammerer, G. & Herskowitz, I. FAR1 links the signal transduction pathway to the cell cycle machinery in yeast. *Cell* **73,** 747–760 (1993).
16. McKinney, J. D., Chang, F., Heintz, N. & Cross, F. R. Negative regulation of FAR1 at the Start of the yeast cell cycle. *Genes & Development* **7,** 833–843 (1993).
17. Durandau, E., Aymoz, D. & Pelet, S. Dynamic single cell measurements of kinase activity by synthetic kinase activity relocation sensors. *BMC Biol.* **13,** 55 (2015).
18. Conlon, P., Gelin-Licht, R., Ganesan, A., Zhang, J. & Levchenko, A. Single-cell dynamics and variability of MAPK activity in a yeast differentiation pathway. *Proc Natl Acad Sci USA* **113,** E5896–E5905 (2016).
19. Doncic, A. *et al.* Compartmentalization of a bistable switch enables memory to cross a feedback-driven transition. *Cell* **160,** 1182–1195 (2015).
20. Reményi, A., Good, M. C., Bhattacharyya, R. P. & Lim, W. A. The role of docking interactions in mediating signaling input, output, and discrimination in the yeast MAPK network. *Mol Cell* **20,** 951–962 (2005).
21. Pelet, S., Dechant, R., Lee, S. S., van Drogen, F. & Peter, M. An integrated image analysis platform to quantify signal transduction in single cells. *Integrative biology : quantitative biosciences from nano to macro* **4,** 1274–1282 (2012).
22. Bean, J. M., Siggia, E. D. & Cross, F. R. Coherence and timing of cell cycle start examined at single-cell resolution. *Mol Cell* **21,** 3–14 (2006).
23. Doncic, A., Falleur-Fettig, M. & Skotheim, J. M. Distinct interactions select and maintain a specific cell fate. *Mol Cell* **43,** 528–539 (2011).
24. Costanzo, M. *et al.* CDK activity antagonizes Whi5, an inhibitor of G1/S transcription in yeast. *Cell* **117,** 899–913 (2004).
25. de Bruin, R. A. M., McDonald, W. H., Kalashnikova, T. I., Yates, J. & Wittenberg, C. Cln3 activates G1-specific transcription via phosphorylation of the SBF bound repressor Whi5. *Cell* **117,** 887–898 (2004).
26. Charvin, G., Cross, F. R. & Siggia, E. D. A microfluidic device for temporally controlled gene expression and long-term fluorescent imaging in unperturbed dividing yeast cells. *PLoS ONE* **3,** e1468 (2008).
27. Yu, R. C. *et al.* Negative feedback that improves information transmission in yeast signalling. *Nature* **456,** 755–761 (2008).
28. Vaga, S. *et al.* Phosphoproteomic analyses reveal novel cross-modulation mechanisms between two signaling pathways in yeast. *Molecular Systems Biology* **10,** 767 (2014).
29. Hao, N., Yildirim, N., Wang, Y., Elston, T. C. & Dohlman, H. G. Regulators of G protein signaling and transient activation of signaling: experimental and computational analysis reveals negative and positive feedback controls on G protein activity. *J Biol Chem* **278,** 46506–46515 (2003).
30. Nagiec, M. J. *et al.* Signal inhibition by a dynamically regulated pool of monophosphorylated MAPK. *Mol Biol Cell* **26,** 3359–3371 (2015).
31. Bhattacharyya, R. P. *et al.* The Ste5 scaffold allosterically modulates signaling output of the yeast mating pathway. *Science* **311,** 822–826 (2006).
32. Shou, W. Y. *et al.* Exit from mitosis is triggered by Tem1-dependent release of the protein phosphatase Cdc14 from nucleolar RENT complex. *Cell* **97,** 233–244 (1999).
33. Visintin, R., Hwang, E. S. & Amon, A. Cfi1 prevents premature exit from mitosis by anchoring Cdc14

phosphatase in the nucleolus. *Nature* **398,** 818–823 (1999).
34. Hartwell, L. H., Culotti, J., Pringle, J. R. & Reid, B. J. Genetic control of the cell division cycle in yeast. *Science* **183,** 46–51 (1974).
35. Dirick, L., Böhm, T. & Nasmyth, K. Roles and regulation of Cln-Cdc28 kinases at the start of the cell cycle of Saccharomyces cerevisiae. *EMBO J* **14,** 4803–4813 (1995).
36. Chang, F. & Herskowitz, I. Identification of a gene necessary for cell cycle arrest by a negative growth factor of yeast: FAR1 is an inhibitor of a G1 cyclin, CLN2. *Cell* **63,** 999–1011 (1990).
37. Tyers, M. & Futcher, B. Far1 and Fus3 link the mating pheromone signal transduction pathway to three G1-phase Cdc28 kinase complexes. *Mol Cell Biol* **13,** 5659–5669 (1993).
38. Bishop, A. C. *et al.* A chemical switch for inhibitor-sensitive alleles of any protein kinase. *Nature* **407,** 395–401 (2000).
39. Bhaduri, S. & Pryciak, P. M. Cyclin-specific docking motifs promote phosphorylation of yeast signaling proteins by G1/S Cdk complexes. *Curr Biol* **21,** 1615–1623 (2011).
40. Aymoz, D., Wosika, V., Durandau, E. & Pelet, S. Real-time quantification of protein expression at the single-cell level via dynamic protein synthesis translocation reporters. *Nature Communications* **7,** 11304 (2016).
41. Aymoz, D. *et al.* Timing of gene expression in a cell-fate decision system. *bioRxiv* (2017). doi:10.1101/197103
42. Oda, Y., Huang, K., Cross, F. R., Cowburn, D. & Chait, B. T. Accurate quantitation of protein expression and site-specific phosphorylation. *Proc Natl Acad Sci USA* **96,** 6591–6596 (1999).
43. Wu, C., Leeuw, T., Leberer, E., Thomas, D. Y. & Whiteway, M. Cell cycle- and Cln2p-Cdc28p-dependent phosphorylation of the yeast Ste20p protein kinase. *J Biol Chem* **273,** 28107–28115 (1998).
44. Oehlen, L. J. & Cross, F. R. Potential regulation of Ste20 function by the Cln1-Cdc28 and Cln2-Cdc28 cyclin-dependent protein kinases. *J Biol Chem* **273,** 25089–25097 (1998).
45. Cherkasova, V., Lyons, D. M. & Elion, E. A. Fus3p and Kss1p control G1 arrest in Saccharomyces cerevisiae through a balance of distinct arrest and proliferative functions that operate in parallel with Far1p. *Genetics* **151,** 989–1004 (1999).
46. Oehlen, L. J., Jeoung, D. I. & Cross, F. R. Cyclin-specific START events and the G1-phase specificity of arrest by mating factor in budding yeast. *Mol. Gen. Genet.* **258,** 183–198 (1998).
47. Tyers, M. The cyclin-dependent kinase inhibitor p40SIC1 imposes the requirement for Cln G1 cyclin function at Start. *Proc Natl Acad Sci USA* **93,** 7772–7776 (1996).
48. Meloche, S. & Pouysségur, J. The ERK1/2 mitogen-activated protein kinase pathway as a master regulator of the G1- to S-phase transition. *Oncogene* **26,** 3227–3239 (2007).
49. Davies, H. *et al.* Mutations of the BRAF gene in human cancer. *Nature* **417,** 949–954 (2002).
50. Marshall, C. J. Specificity of Receptor Tyrosine Kinase Signaling - Transient Versus Sustained Extracellular Signal-Regulated Kinase Activation. *Cell* **80,** 179–185 (1995).
51. Pumiglia, K. M. & Decker, S. J. Cell cycle arrest mediated by the MEK/mitogen-activated protein kinase pathway. *Proc Natl Acad Sci USA* **94,** 448–452 (1997).
52. Orford, K. W. & Scadden, D. T. Deconstructing stem cell self-renewal: genetic insights into cell-cycle regulation. *Nat Rev Genet* **9,** 115–128 (2008).
53. Wosika, V. *et al.* New families of single integration vectors and gene tagging plasmids for genetic manipulations in budding yeast. *Molecular Genetics and Genomics* **291,** 2231–2240 (2016).
54. Longtine, M. S. *et al.* Additional modules for versatile and economical PCR-based gene deletion and modification in Saccharomyces cerevisiae. *Yeast* **14,** 953–961 (1998).
55. Goldstein, A. L. & McCusker, J. H. Three new dominant drug resistance cassettes for gene disruption in Saccharomyces cerevisiae. *Yeast* **15,** 1541–1553 (1999).
56. Edelstein, A., Amodaj, N., Hoover, K., Vale, R. & Stuurman, N. Computer control of microscopes using µManager. *Curr Protoc Mol Biol* **Chapter 14,** Unit14.20 (2010).

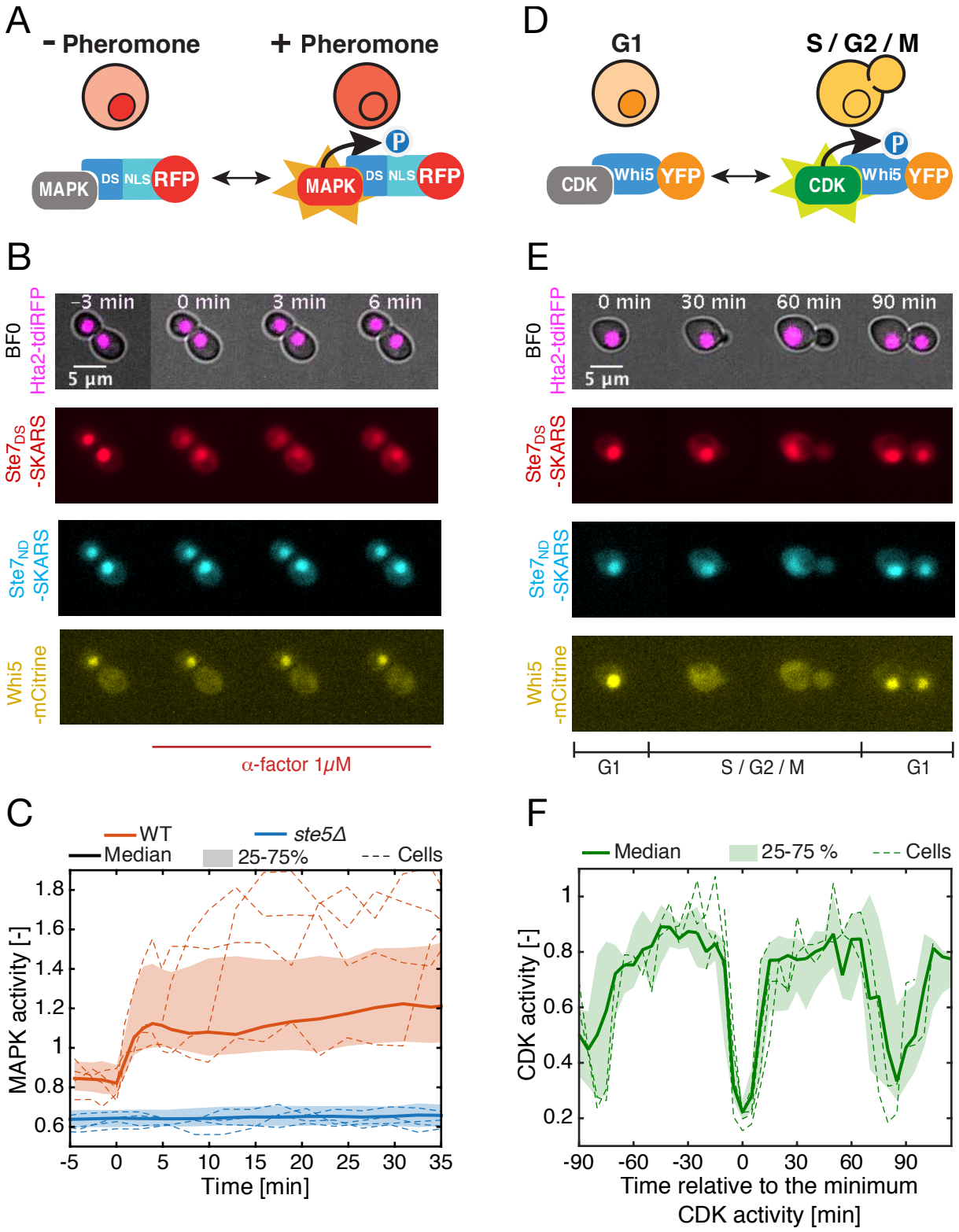
A
- Pheromone
+ Pheromone
MAPK
DS
NLS
RFP
P
B
BF0
Hta2-tdiRFP
-3 min
0 min
3 min
6 min
5 µm
Ste7DS -SKARS
Ste7ND -SKARS
Whi5 -mCitrine
α-factor 1µM
C
WT
ste5Δ
Median
25-75%
Cells
MAPK activity [-]
Time [min]
D
G1
S / G2 / M
CDK
Whi5
YFP
E
0 min
30 min
60 min
90 min
G1
S / G2 / M
F
Median
25-75 %
Cells
CDK activity [-]
Time relative to the minimum CDK activity [min]

Figure 1

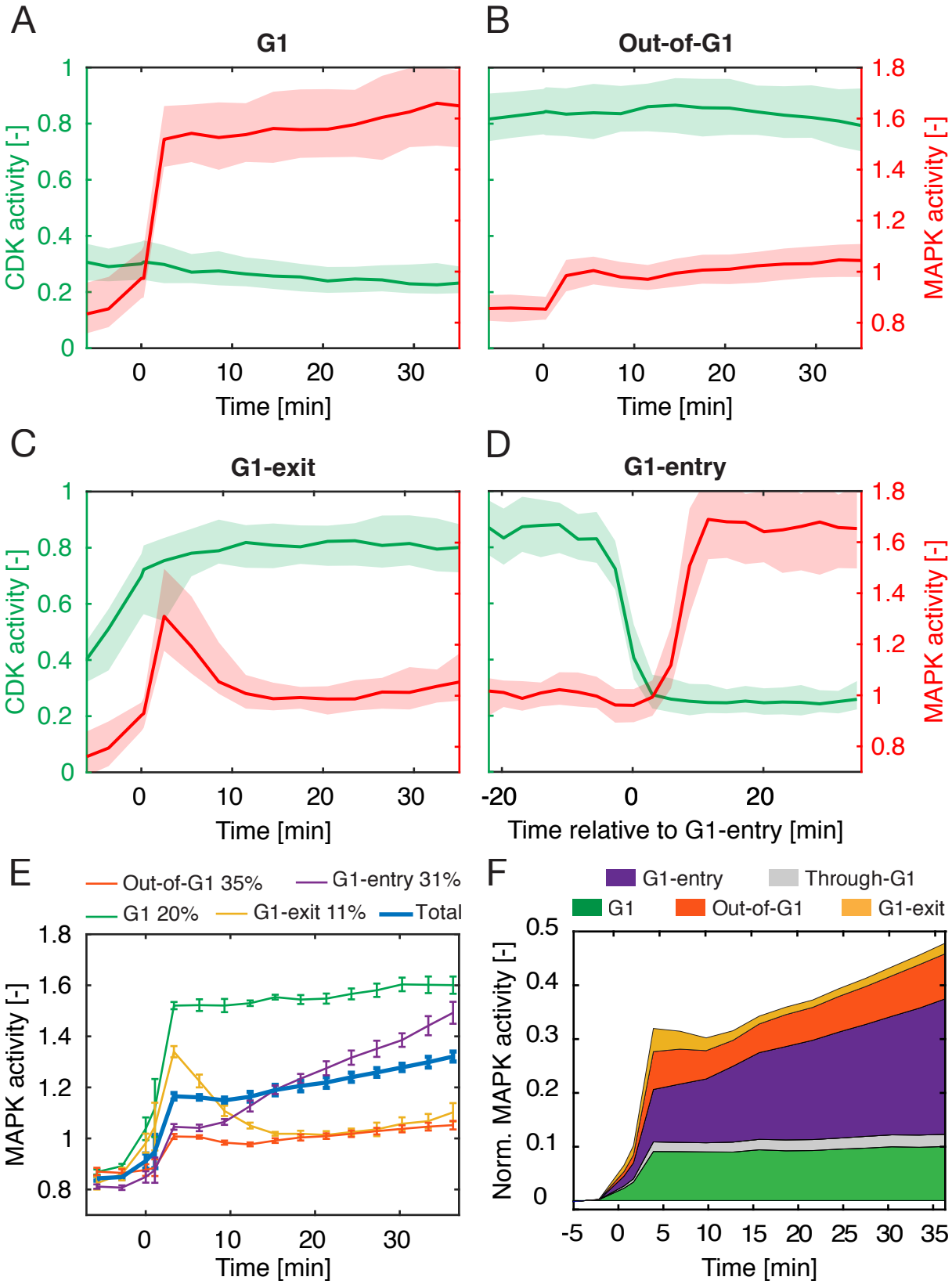
A
G1
CDK activity [-]
MAPK activity [-]
Time [min]
B
Out-of-G1
Time [min]
C
G1-exit
Time [min]
D
G1-entry
Time relative to G1-entry [min]
E
Out-of-G1 35%
G1-entry 31%
G1 20%
G1-exit 11%
Total
MAPK activity [-]
Time [min]
F
G1-entry
Through-G1
G1
Out-of-G1
G1-exit
Norm. MAPK activity [-]
Time [min]

Figure 2

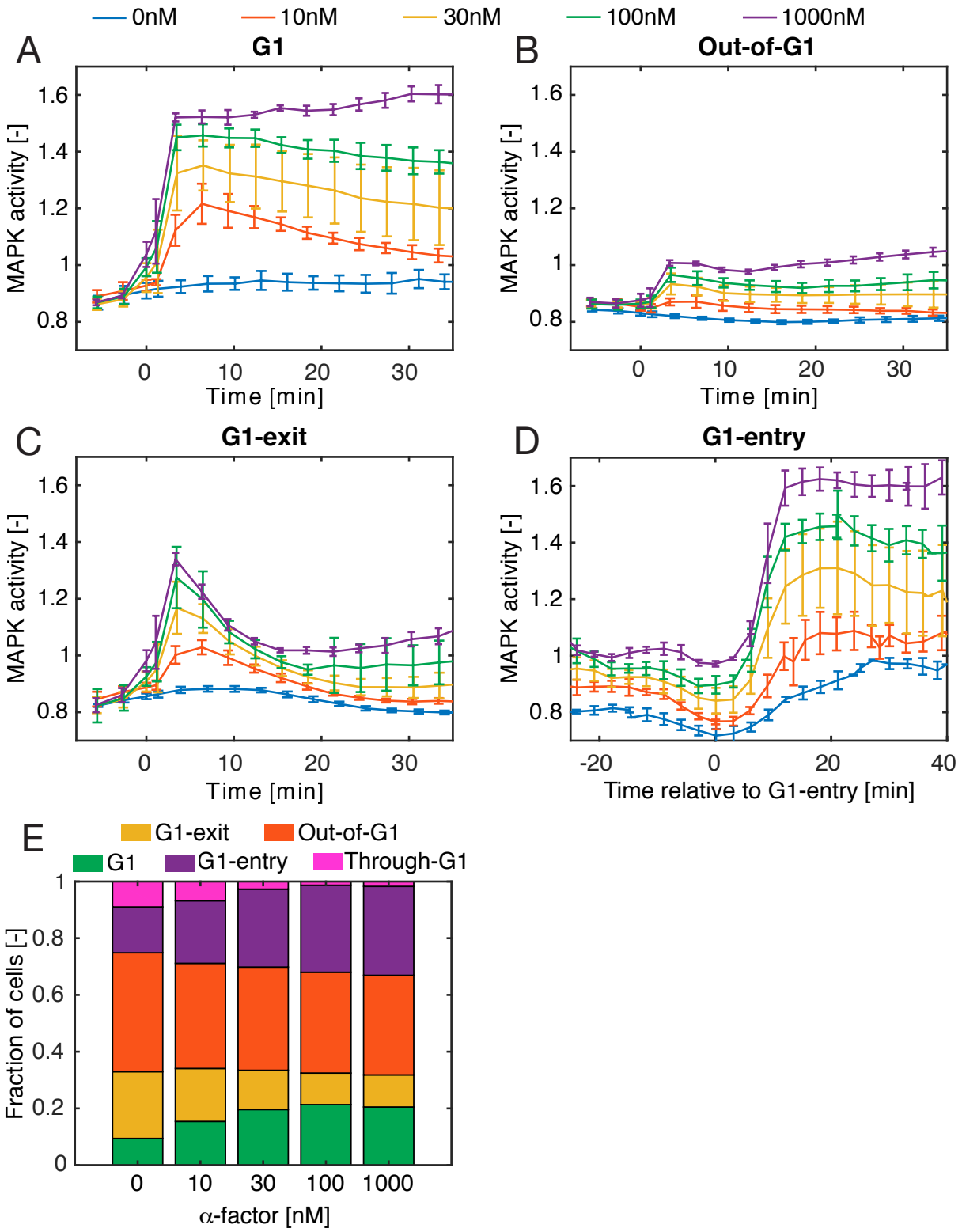
0nM
10nM
30nM
100nM
1000nM
A
G1
B
Out-of-G1
C
G1-exit
D
G1-entry
MAPK activity [-]
Time [min]
Time relative to G1-entry [min]
E
G1-exit
Out-of-G1
G1
G1-entry
Through-G1
Fraction of cells [-]
α-factor [nM]

Figure 3

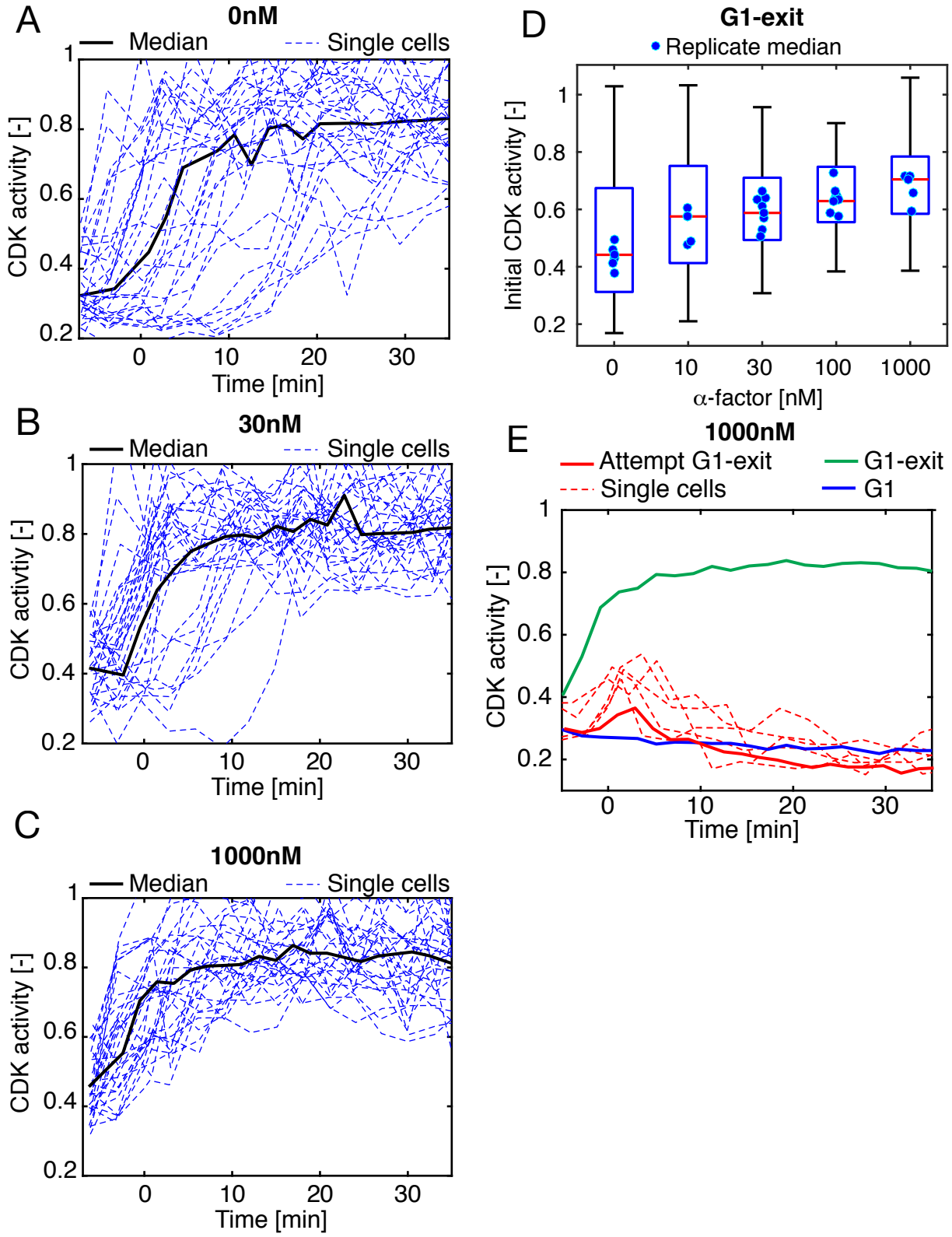
A
0nM
Median
Single cells
CDK activity [-]
Time [min]
B
30nM
Median
Single cells
CDK activity [-]
Time [min]
C
1000nM
Median
Single cells
CDK activity [-]
Time [min]
D
G1-exit
Replicate median
Initial CDK activity [-]
α-factor [nM]
E
1000nM
Attempt G1-exit
Single cells
G1-exit
G1
CDK activity [-]
Time [min]

Figure 4

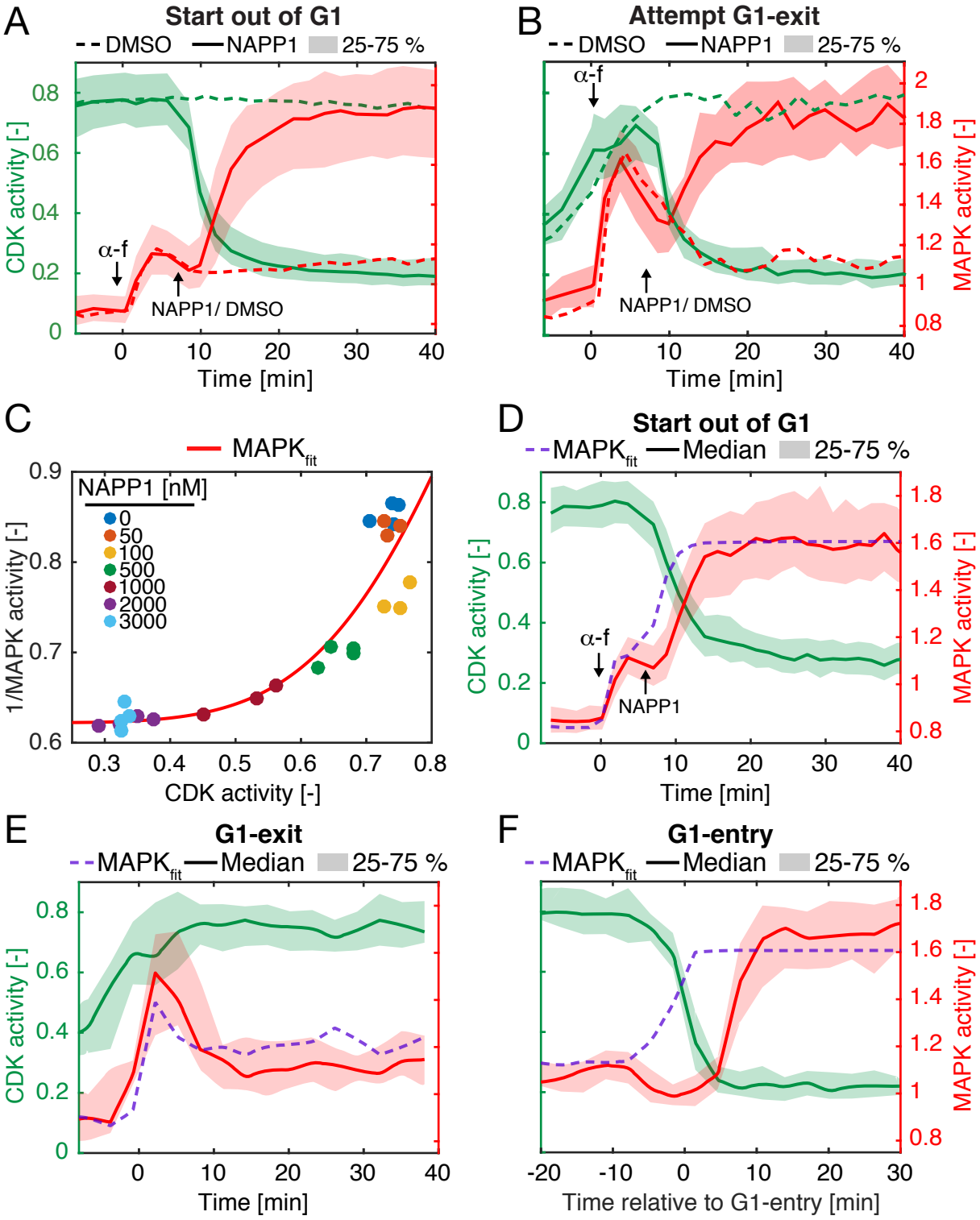
A
Start out of G1
DMSO
NAPP1
25-75 %
CDK activity [-]
α-f
NAPP1/ DMSO
Time [min]
B
Attempt G1-exit
DMSO
NAPP1
25-75 %
α-f
NAPP1/ DMSO
MAPK activity [-]
Time [min]
C
MAPK$_{fit}$
NAPP1 [nM]
0
50
100
500
1000
2000
3000
1/MAPK activity [-]
CDK activity [-]
D
Start out of G1
MAPK$_{fit}$
Median
25-75 %
CDK activity [-]
α-f
NAPP1
MAPK activity [-]
Time [min]
E
G1-exit
MAPK$_{fit}$
Median
25-75 %
CDK activity [-]
Time [min]
F
G1-entry
MAPK$_{fit}$
Median
25-75 %
MAPK activity [-]
Time relative to G1-entry [min]

Figure 5

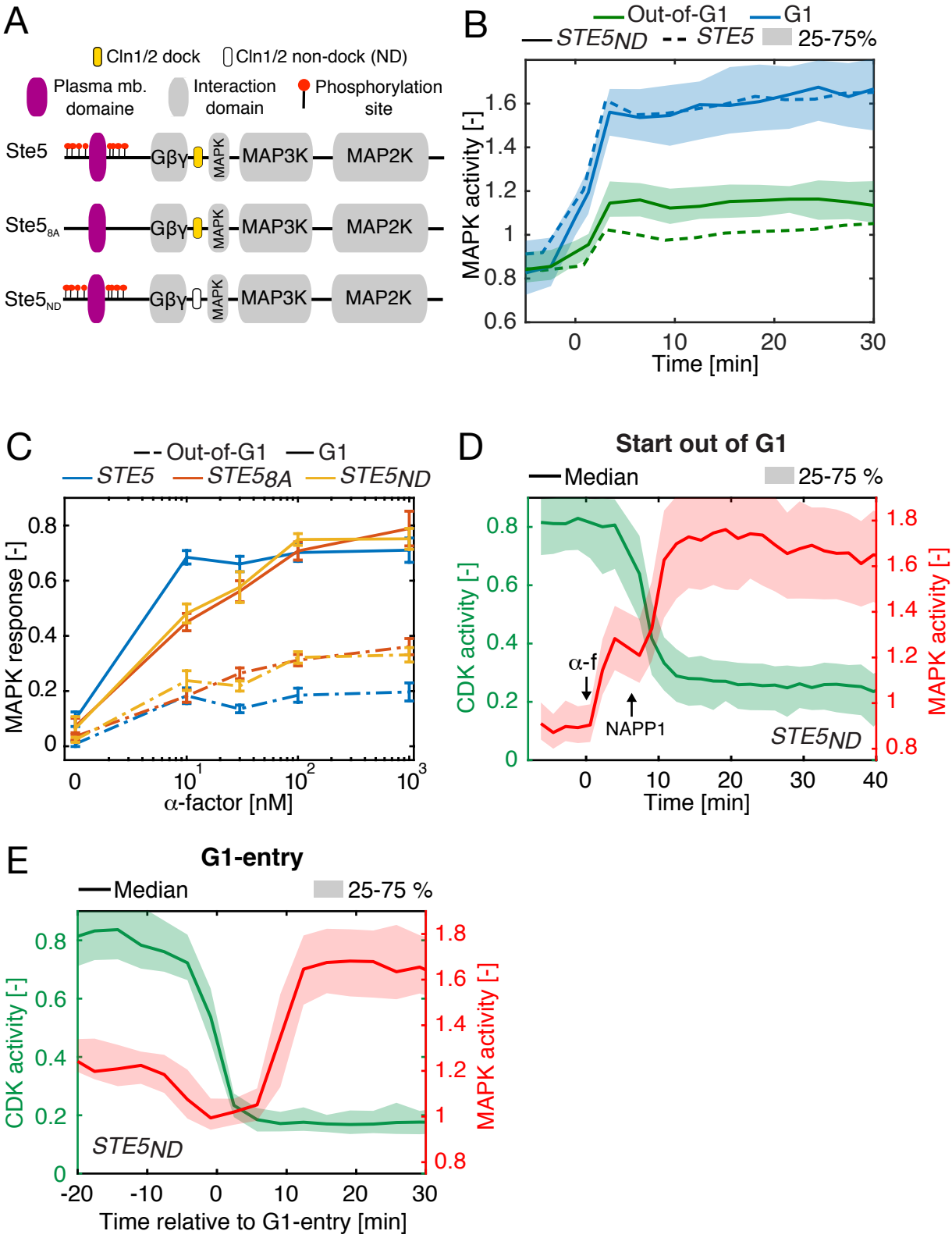
A
Cln1/2 dock
Cln1/2 non-dock (ND)
Plasma mb. domaine
Interaction domain
Phosphorylation site
Ste5
Ste5$_{8A}$
Ste5$_{ND}$
Gβγ
MAPK
MAP3K
MAP2K
B
Out-of-G1
G1
STE5ND
STE5
25-75%
MAPK activity [-]
Time [min]
C
Out-of-G1
G1
STE5
STE5$_{8A}$
STE5ND
MAPK response [-]
α-factor [nM]
D
Start out of G1
Median
25-75 %
CDK activity [-]
MAPK activity [-]
α-f
NAPP1
STE5ND
Time [min]
E
G1-entry
Median
25-75 %
CDK activity [-]
MAPK activity [-]
STE5ND
Time relative to G1-entry [min]

Figure 6

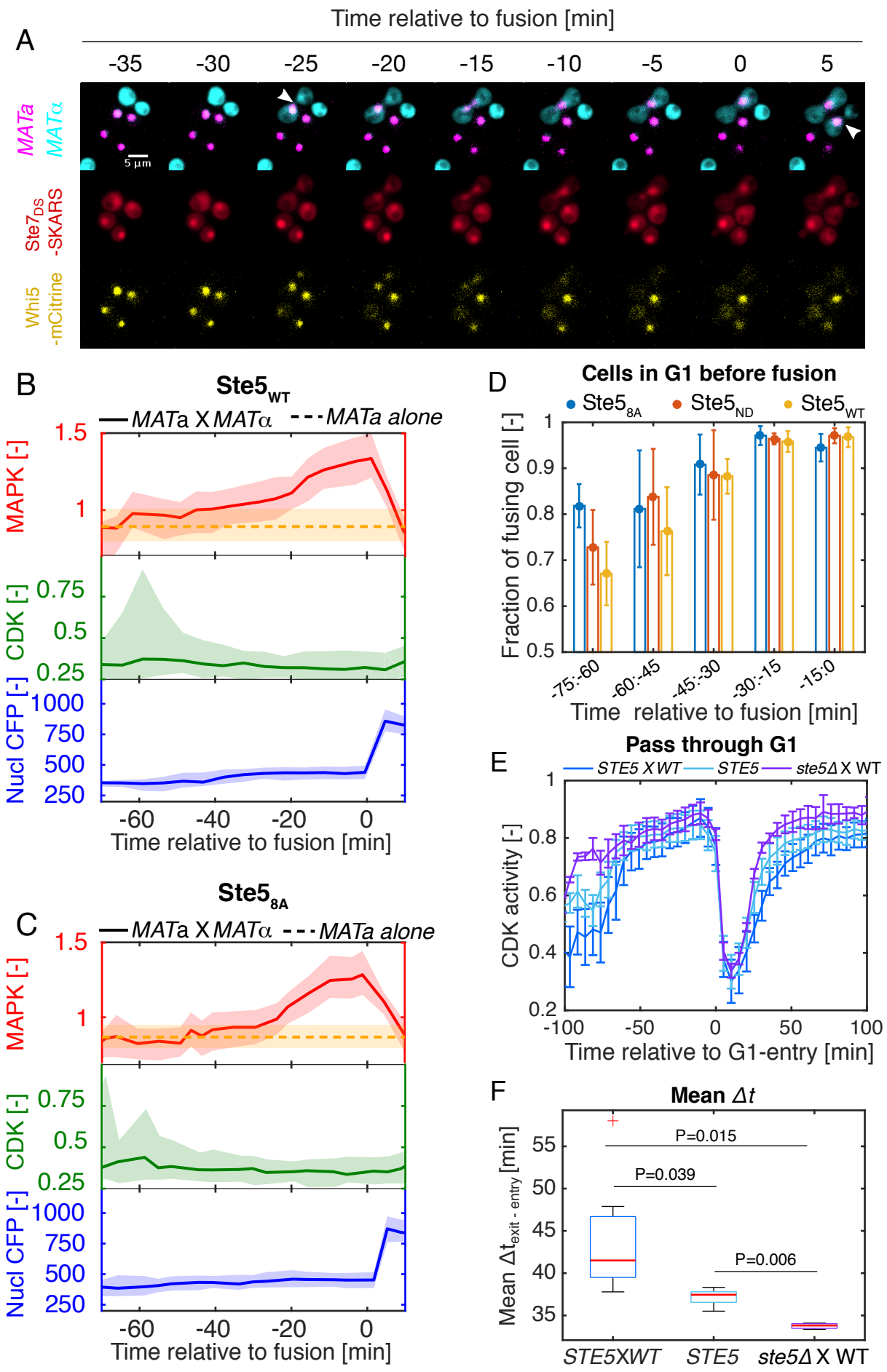
A
Time relative to fusion [min]
-35
-30
-25
-20
-15
-10
-5
0
5
MATa
MATα
5 µm
Ste7DS -SKARS
Whi5 -mCitrine
B
Ste5WT
MATa X MATα
MATa alone
MAPK [-]
CDK [-]
Nucl CFP [-]
Time relative to fusion [min]
C
Ste5 8A
MATa X MATα
MATa alone
MAPK [-]
CDK [-]
Nucl CFP [-]
Time relative to fusion [min]
D
Cells in G1 before fusion
Ste5 8A
Ste5 ND
Ste5 WT
Fraction of fusing cell [-]
-75:-60
-60:-45
-45:-30
-30:-15
-15:0
Time relative to fusion [min]
E
Pass through G1
STE5 X WT
STE5
ste5Δ X WT
CDK activity [-]
Time relative to G1-entry [min]
F
Mean Δt
P=0.015
P=0.039
P=0.006
Mean Δt exit - entry [min]
STE5XWT
STE5
ste5Δ X WT

Figure 7